Journal of Materials Chemistry A

PAPER

View Article Online
View Journal | View Issue

Cite this: J. Mater. Chem. A, 2017, 5, 712

A wide band gap polymer based on indacenodithieno[3,2-*b*]thiophene for high-performance bulk heterojunction polymer solar cells†

Woosung Lee[a] and Jae Woong Jung*[b]

Received 3rd October 2016
Accepted 23rd November 2016

DOI: 10.1039/c6ta08591a

www.rsc.org/MaterialsA

Although wide band gap polymers have attracted much interest for applications in polymer solar cells (PSCs) as short-wavelength light absorbers in tandem devices, the power conversion efficiencies (PCEs) of wide band gap polymer-based single cell devices are inferior to those of narrow-band gap polymers due to their restricted light absorption range. Thus, it is necessary to develop new semiconducting polymers for optimal device performance. Herein, a new wide band gap polymer (PIDTT-TT) was designed and synthesized by copolymerizing indacenodithieno[3,2-*b*]thiophene (IDTT) with thieno[3,2-*b*]thiophene (TT), resulting in a wide band gap polymer (PIDTT-TT) with an absorption onset at ~580 nm (optical band gap = 2.14 eV). Electrochemical investigations indicated the low-lying energy levels (HOMO = −5.35 eV) of PIDTT-TT compared to those of P3HT (HOMO = 5.00 eV), which is beneficial for obtaining a high open-circuit voltage (V_{OC}) in the device. The optimized morphology of the PIDTT-TT:$PC_{71}BM$ blend film led to a high V_{OC} (0.96 V) and fill factor (FF) (0.66), which compensate for the limited light absorption range, achieving a power conversion efficiency (PCE) of 7.10%. Furthermore, the deep energy levels of PIDTT-TT reinforced the air stability of the solar cell, which retained 85% of its initial PCE after being stored for 120 h under ambient conditions. Accordingly, PIDTT-TT is a potential candidate for applications in tandem solar cells. This study enriched the design rules of wide band gap polymers for high-performance PSCs.

Introduction

Tremendous efforts have been devoted to the investigation of solar cells as a next-generation photovoltaic technology because they can generate electricity from sunlight at a very low cost.[1–4] Among them, polymer solar cells (PSCs), which have been emerging as an environmentally benign technology with the ability to convert solar energy into electricity, are attractive due to their low material cost and light, soft, and flexible properties.[5–10] Significant advances, such as new material development, device engineering, and processing optimization, have been made in the field of PSCs, and their photovoltaic performance has been rapidly improved in recent years.[11–14] In particular, remarkable progress has been made with p-type conjugated polymers to help boost the power conversion efficiency (PCE) of PSCs to ~10% over the last few years.[15–17]

Currently, most p-type conjugated polymers for solar cell applications are designed to be low band gap (E_g) materials; thus, they exhibit an extended absorption range in the NIR region for enlarged light absorption and increased short-circuit current density (J_{SC}) in devices.[18] The most facile approach used to design the low band gap polymers employs push–pull-type alternating copolymers consisting of electron-donating (D) and electron-accepting (A) units in one polymer backbone.[19,20] Although D–A-type low band gap polymers have been shown to be successful in lowering the band gap of conjugated polymers *via* internal charge transfer, they generally suffer from an increased highest occupied molecular orbital (HOMO) level, which results in a limited open-circuit voltage (V_{OC}) of the device. Additionally, the intrinsic narrow absorption bands of low band gap polymers limit broad photon harvesting, preventing full utilization of the entire solar spectrum.[21]

So far, unlike low band gap polymers, wide band gap polymers have been overlooked for solar cell applications since they only absorb photons in a restricted range below 650 nm (E_g > 2.0 eV). However, they are still of importance for PSCs, because the wide band gap polymers usually exhibit deep

[a]ICT Textile & Apparel R&D Group, Korea Institute of Industrial Technology (KITECH), 143 Hanggaulro, Sangnokgu, Ansan-si, Gyeonggi-do 426-910, Republic of Korea
[b]Department of Advanced Materials Engineering for Information & Electronics, Kyung Hee University, 1732 Deogyeong-daero, Giheung-gu, Yongin-si, Gyeonggi-do 446-701, Republic of Korea. E-mail: wodndwjd@khu.ac.kr

† Electronic supplementary information (ESI) available: Thermal analysis, carrier mobility, *J–V* curve and IPCE for P3HT:$PC_{71}BM$-based devices. See DOI: 10.1039/c6ta08591a

energy levels (low-lying HOMO level) that favour higher V_{OC} of devices.[22,23] In addition, wide band gap polymers can be used as a vital component (*i.e.*, the short wavelength photoactive layer) in tandem devices, that makes the tandem PSCs absorb a wide range of solar spectrum.[24–26] Until now, one of the most widely used wide band gap polymer is poly(3-hexylthiophene) (P3HT). Although P3HT possesses intense UV-Vis absorption to ~620 nm (E_g = 2.0 eV), high crystallinity and good charge mobility, a relatively high-lying HOMO level (~−5.1 eV) limits the V_{OC} of the derived device to ~0.6 V with the $PC_{61}BM$ acceptor.[27,28] Alternatively, several different conjugated moieties such as carbazole,[29] anthracene[30] or benzo[1,2-*b*:4,5-*b*′]dithiophene[31] have been used to construct wide band gap polymers. These wide band gap polymers usually absorb photons in the UV-Vis region, showing lowered HOMO levels, amenable to larger V_{OC} and thus high PCEs in the devices.

Indacenodithieno[3,2-*b*]thiophene (IDTT) is another interesting moiety that can be used to construct conjugated polymers.[32] The covalently forced coplanar structure of IDTT enlarges the effective conjunction in the IDTT-based polymer backbone. The multi-fused, seven-membered entity facilitates the overlap of π-orbitals along the polymer backbone. Also, the thieno[3,2-*b*]thiophene-flanked fully aromatic coplanar conjugation consisting of a heterocyclic aromatic system effectively lowers the energetic disorder, which facilitates strong intermolecular interactions and improved charge transport.[33] The highly conjugated nature of IDTT-based polymers leads to a coplanar and rigid polymer backbone, resulting in a low energetic disorder and thus efficient charge transport along the polymer backbone.[34] Recently, IDTT has been demonstrated as a core building block of high-performance conjugated polymers designed to achieve high mobility in organic field-effect transistor (OFET) devices and PSCs.[35–38] More importantly, IDTT is a fused polycyclic acene, which effectively reduces the electron-richness; thus, IDTT-based polymers exhibit relatively deep HOMO levels with enhanced V_{OC}s compared to P3HT, suggesting its potential as a building block for wide band gap polymers.[39–41] However, there have been few reports investigating IDTT-based wide band gap polymers with PCE >7%.[42]

In this study, we aim to explore a new conjugated polymer with an enlarged band gap for efficient PSCs. We report a wide band gap polymer, PIDTT-TT, that employs IDTT and thieno[3,2-*b*]thiophene (TT) in the polymer backbone. Due to the strong electron-donating capabilities of IDTT and TT, PIDTT-TT is a D–D′ type alternating copolymer; this is in contrast to D–A type low band gap polymers. It should be highlighted that the D–D′ type PIDTT-TT exhibits a wide band gap (E_g = 2.14 eV) with deep energy levels. Also, PIDTT-TT has an enhanced extinction coefficient compared to P3HT, which can compensate for the limited absorption range of wide band gap polymers. By careful optimization of the photoactive layer film morphology, PIDTT-TT achieved a PCE of 7.10%, which is one of the highest PCE values reported to date for the wide band gap polymers. Significantly, the device based on PIDTT-TT displayed increased ambient stability compared to P3HT; this mainly arises from the deep energy levels of PIDTT-TT, suggesting that it may be a promising candidate for use in highly stable PSCs that utilize wide band gap polymers.

Experimental section

Materials and characterization

All the solvents and reagents were purchased from commercial sources (Aldrich, TCI and Acros). DMF and toluene were dried over activated molecular sieves (3 Å) and stored under a N_2 atmosphere. $Pd(PPh_3)_4$ was stored under dark conditions in an N_2 atmosphere before use. [6,6]-Phenyl-C_{71}-butyric acid methyl ester ($PC_{71}BM$) was purchased from Nano-C. All other reagents were purchased from Sigma-Aldrich unless specified and used as received. Gel permeation chromatography (GPC) calibrated by polystyrene standards was carried out to determine the molecular weight of PIDTT-TT using *o*-dichlorobenzene (DCB) as an eluent. The optical absorption spectra were obtained by using an UV-Vis spectrophotometer (Lambda 25, Perkin Elmer). Cyclic voltammetry was conducted on a potentiostat/galvanostat (VMP 3, Biologic) in $(CH_3CH_2CH_2CH_2)_4N(PF_6)$ (0.1 M) as the supporting electrolyte in acetonitrile with a Pt working electrode, a platinum-wire counter electrode and a Ag/AgCl reference electrode. A thin film of PIDTT-TT was cast on an ITO-coated substrate for fabrication of a working electrode. Density functional theory (DFT) calculations for the repeating units of PIDTT0TT was carried out on a Gaussian 03W at the B3LYP/6-31G(d,p) level. The morphologies of the blend films were observed by transmission electron microscopy (TEM) (JEM-1010, JEOL) operating in 80 kV of acceleration voltage by floating the blend film onto the Cu grid after immersing the device in deionized water.

Synthesis of PIDTT-TT

A mixture of 2,6-bis(trimethylstannyl)4,9-di(*p*-hexyl-phenyl) indacenodithieno[3,2-*b*]thiophene (M1) (134.6 mg, 0.10 mmol) and 2,5-dibromothieno[3,2-*b*]thiophene (M2) (29.8.0 mg, 0.10 mmol) was dissolved in an anhydrous toluene (3.5 mL) under nitrogen conditions. After 4 mg of $Pd(PPh_3)_4$ was quickly added to the mixture, it was flushed with nitrogen for 10 min. The mixture was then refluxed for 72 h, followed by subsequent addition of 35 μL of 2-bromothiophene and 50 μL of 2-tributylstannylthiophene with an interval of 12 h for end-capping. After further reflux for 24 h, the mixture was poured into methanol. The precipitate was filtered through a Soxhlet thimble and then subjected to Soxhlet extraction successively with methanol, acetone, hexane, ethyl acetate and ethyl ether. The residue in the thimble filter was collected. The solid was completely dried under vacuum for 12 h to yield PIDTT-TT as a dark red powder (95 mg, Y = 68%).

^{1}H NMR (500 MHz, $CDCl_3$): 8.40–8.10 (m, 2H), 7.80–6.60 (m, 20H), 4.10–0.75 (m, 52H). Anal. calc. for $C_{76}H_{80}S_6$: C, 76.98; H, 6.80; S, 16.22. Found: C, 76.75; H, 6.84; S, 16.40.

Device fabrication and test

Solar cell devices were fabricated with an inverted configuration of ITO/ZnO/PEIE/PIDTT-TT:$PC_{71}BM$/MoO_3/Ag.[43] Onto the pre-cleaned ITO substrate, ZnO (30 nm) was spin-coated from ZnO

precursor solution (zinc acetate dihydrate in 2-methoxyethanol and ethanolamine) and then annealed at 200 °C for 1 h. A thin layer of PEIE was spin coated onto the ZnO film from dilute PEIE solution (0.4 wt% in 2-methoxyethanol) at 5000 rpm for 1 min and dried at 100 °C for 10 min. The active layers were then spin-coated from the blend solution of PIDTT-TT and $PC_{71}BM$ (3 wt% in DCB with or without different amounts of additives) at 1400 rpm for 90 s to form a ~280 nm thick film. In order to control the solvent evaporation rate, the wet film was further kept in closed jar for 2 h. The device fabrication was completed by thermal evaporation of MoO_3 (8 nm) and Ag (150 nm) under vacuum (<10^{-6} Torr). The active area (0.04 cm^2) of the device was defined by a shadow mask. The device employing P3HT:$PC_{71}BM$ was fabricated by spin coating the blend solution of P3HT and $PC_{71}BM$ (1 : 0.9 w/w, 38 mg mL^{-1} in DCB with 2 vol% of 1-chloronaphthalene). More than 20 solar cell devices are fabricated for each condition. The film thickness of the active layer was measured by atomic force microscopy (Park systems). The current density–voltage (J–V) characteristics were measured with a Keithley 2400 source-meter under AM 1.5G (100 mW cm^{-2}) simulated by using a Newport-Oriel solar simulator. The light intensity was calibrated using a NREL-certified photodiode prior to measurement. The incident photon-to-current efficiency (IPCE) was measured using a lock-in amplifier with a current preamplifier at the short circuit current state under illumination of monochromatic light. The champion devices were stored under ambient conditions in the dark for ambient stability investigation. The single carrier mobility was calculated from J–V curves obtained under dark conditions using hole-only (ITO/PEDOT:PSS/PIDTT-TT:$PC_{71}BM$/MoO_3/Ag) and electron-only (ITO/ZnO/PEIE/PIDTT-TT:$PC_{71}BM$/PEIE/Ag) devices. The J–V curves were fitted by using the space charge-limited current (SCLC) model using the Mott–Gurney square law, $J = (9/8)\varepsilon_0\varepsilon_r\mu(V^2/L^3)$, where ε_0 is vacuum permittivity, ε_r is the dielectric constant of polymer, μ is the charge carrier mobility, V is the effective applied voltage, and L is the thickness of the BHJ active layer film.

Results and discussion

Fig. 1a describes the synthetic route used to fabricate PIDTT-TT. The monomers (M1 and M2) are prepared as reported elsewhere.[35,37] The polymer was synthesized *via* a palladium-mediated Stille coupling reaction. The number-average molecular weight (M_n) of PIDTT-TT was 32.5 kDa with a polydispersity index (PDI) of 1.87. The polymers were soluble in common organic solvents such as tetrahydrofuran, chloroform, and DCB at room temperature. Thermogravimetric analysis (TGA) measurements were employed to evaluate the thermal stability of the polymer (Fig. S1a†). The decomposition temperature (T_d) was observed to be 398 °C (5% weight loss), which meets the requirements of thermal stability for photovoltaic applications. The differential scanning calorimetry (DSC) results for PIDTT-TT showed no thermal transition from 20 to 300 °C (Fig. S1b†).

The UV-Vis absorption spectra of PIDTT-TT are shown in Fig. 1b. PIDTT-TT exhibits intense absorption between 450 and 580 nm. On the basis of an absorption onset at ~580 nm, the optical band gap of PIDTT-TT is 2.14 eV. The thin film of

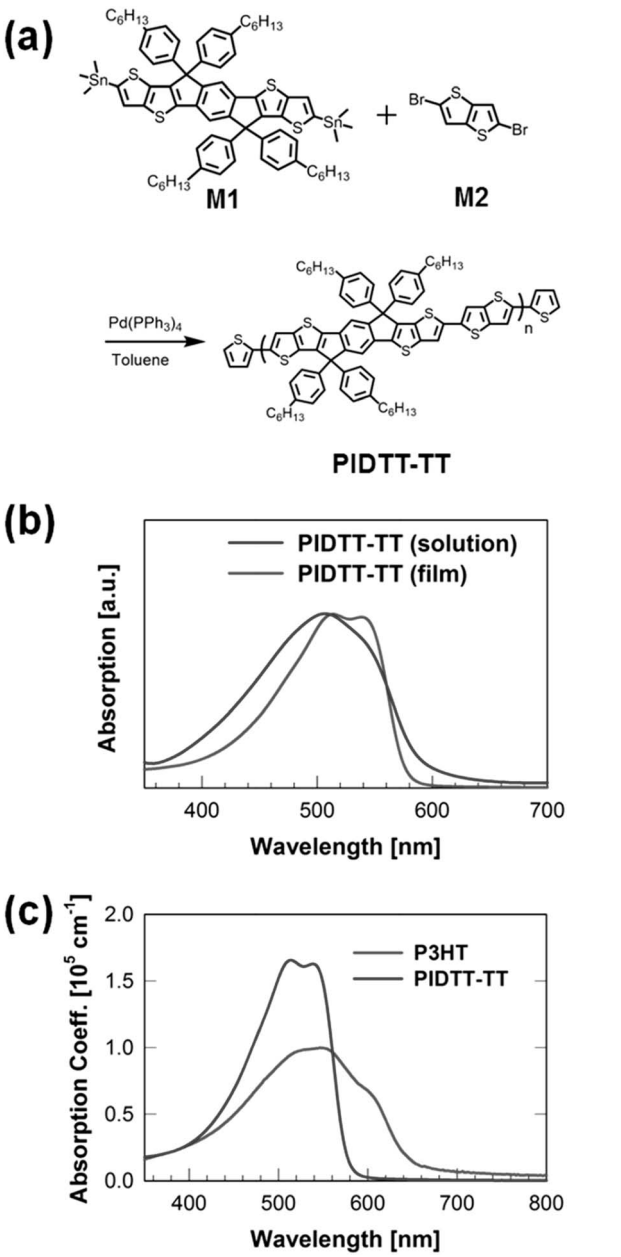

Fig. 1 (a) Synthetic scheme and (b) UV-Vis absorption spectra of PIDTT-TT. (c) Absorption spectra comparison between PIDTT-TT and P3HT.

PIDTT-TT displayed two absorption peaks, which correspond to the π–π* transition and a vibronic peak at 513 and 538 nm, respectively. The dilute solution of PIDTT-TT also exhibited a vibronic shoulder at 535 nm, implying a certain degree of intermolecular packing of the polymer chains in solution. The absorption properties of PIDTT-TT were compared to those of P3HT; the absorption band of PIDTT-TT was significantly blue-shifted relative to P3HT, showing the enlarged band gap of PIDTT-TT compared to P3HT (the UV-Vis absorption spectra of the solution of PIDTT-TT and P3HT are shown in Fig. S2†). More interestingly, the extinction coefficient of PIDTT-TT was 1.7 × 10^5 cm^{-1}, which is 70% higher than that of P3HT (1.0 × 10^5 cm^{-1}).

This suggests that PIDTT-TT would harvest photons more efficiently as compared to P3HT (Fig. 1c).

The energy levels of PITT-TT were measured by electrochemical chemical analysis *via* cyclic voltammetry. The HOMO level of PIDTT-TT was estimated to be −5.35 eV, as estimated from the empirical equation E_{HOMO} (eV) = $-(E_{onset}(ox.) + 4.4)$ (Fig. 2a). We estimated the LUMO level of PIDTT-TT to be −3.21 eV by subtracting the optical band gap from the corresponding HOMO level. Given that the LUMO of $PC_{71}BM$ is −4.10 eV, PIDTT-TT affords a sufficient LUMO offset from $PC_{71}BM$ to drive efficient exciton dissociation and electron transfer within the photoactive layer (Fig. 1b). The molecular orbital distributions at the HOMO and LUMO levels were calculated using density functional theory (DFT). As shown in Fig. 3, the HOMO electrons are delocalized along the polymer backbone, whereas the LUMO electrons are localized on the IDTT unit. This indicates that the TT unit exhibits strong electron-donating capabilities. It should be noted that the well-distributed HOMO and LUMO electrons of PIDTT-TT over the polymer backbone form a quinoidal structure (strong orbital hybridization), which is beneficial for efficient charge transport.

To explore the photovoltaic performance of PIDTT-TT, we fabricated devices with an inverted configuration (ITO/ZnO/PEIE/PIDTT-TT:$PC_{71}BM$/MoO_3/Ag). The *J*–*V* curves of the devices under AM 1.5G illumination are shown in Fig. 4, and the corresponding device parameters are summarized in Table 1. To determine the optimum blend ratio of PIDTT-TT:$PC_{71}BM$, different blend ratios of bulk heterojunction (BHJ) films from

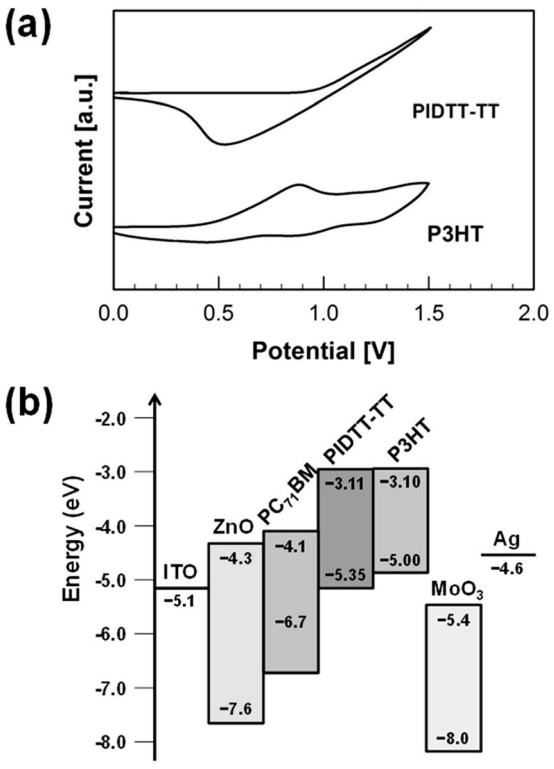

Fig. 2 (a) Cyclic voltammograms and (b) energy level diagram of PIDTT-TT and P3HT.

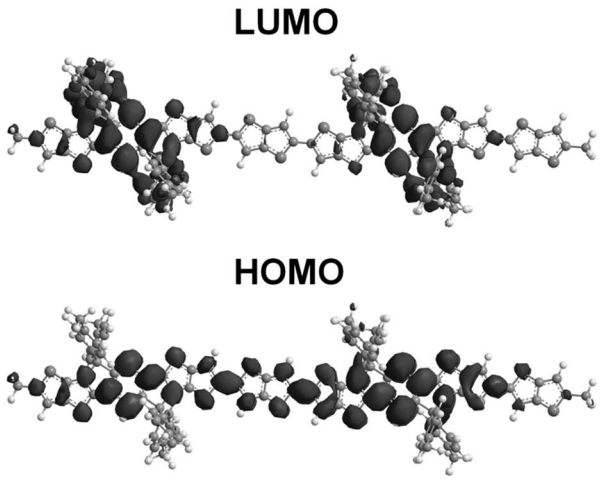

Fig. 3 LUMO (top) and HOMO (bottom) orbital distributions of two repeating units of PIDTT-TT on the optimized molecular structure.

1 : 1 to 1 : 2.5 in DCB were investigated. As shown Fig. 4a, the J_{SC}s of the devices increased from 5.08 mA cm^{-2} (at a 1 : 1 blend ratio) to 7.46 mA cm^{-2} (at a 1 : 1.5 blend ratio) and to 10.15 mA cm^{-2} (at a 1 : 2 blend ratio). However, the J_{SC} decreased to 8.85 mA cm^{-2} at a 1 : 2.5 blend ratio (Table 1). The fill factor (FF) of the device showed a similar trend to the J_{SC}, increasing from the 1 : 1 ratio to 1 : 2 ratio, and then decreasing with increasing $PC_{71}BM$ ratio. All devices showed almost the same V_{OC}, 0.96 V. As a result, the optimized 1 : 2 ratio showed a champion PCE of 5.88% (a champion PCE of 2.88% for the 1 : 1 ratio, a champion PCE of 4.30% for the 1 : 1.5 ratio, a champion PCE of 5.10% for the 1 : 2.5 ratio). The IPCE spectra

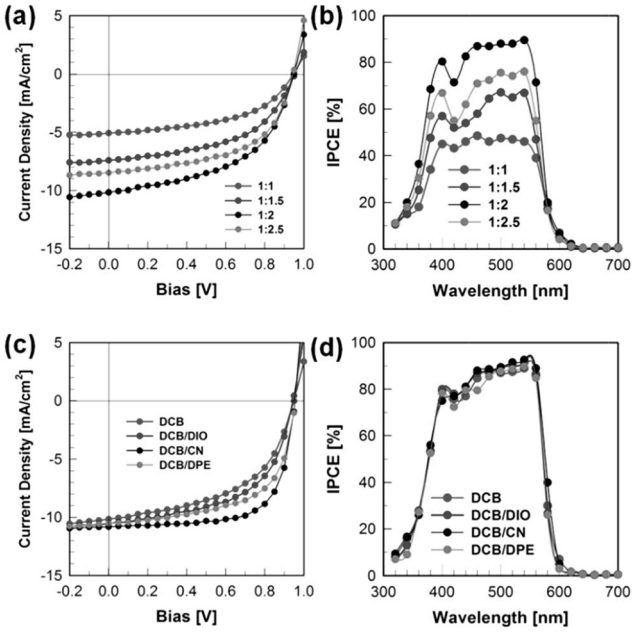

Fig. 4 (a) *J*–*V* curves and (b) corresponding IPCE spectra of the devices of PIDTT-TT:$PC_{71}BM$ with a varied blend ratio. (c) *J*–*V* curves and (d) corresponding IPCE spectra of the devices of PIDTT-TT:$PC_{71}BM$ with a varied solvent.

Table 1 Photovoltaic parameters of devices based on PIDTT-TT:$PC_{71}BM$ as an active layer under different conditions

Weight ratio (w/w)	Additive	V_{OC} [V]	J_{SC} [mA cm^{-2}]	FF	PCE [%]	G_{max} [m^{-3} s^{-1}]
1 : 1	—	0.96 ± 0.01	4.93 ± 0.11	0.59 ± 0.01	2.81 ± 0.08	—
1 : 1.5	—	0.96 ± 0.01	7.26 ± 0.08	0.59 ± 0.02	4.20 ± 0.07	—
1 : 2	—	0.96 ± 0.01	9.94 ± 0.10	0.60 ± 0.01	5.71 ± 0.10	4.52×10^{26}
1 : 2.5	—	0.96 ± 0.01	8.72 ± 0.08	0.59 ± 0.01	4.95 ± 0.12	—
1 : 2	DIO	0.96 ± 0.01	10.25 ± 0.07	0.62 ± 0.01	6.27 ± 0.09	8.95×10^{26}
1 : 2	CN	0.96 ± 0.01	10.96 ± 0.11	0.65 ± 0.02	6.98 ± 0.10	1.08×10^{27}
1 : 2	DPE	0.96 ± 0.01	10.17 ± 0.10	0.61 ± 0.02	6.05 ± 0.09	7.29×10^{26}
1 : 0.9[a]	CN	0.55 ± 0.01	10.16 ± 0.08	0.66 ± 0.01	3.76 ± 0.10	—

[a] Device based on P3HT:$PC_{71}BM$ (see ESI).

showed a photocurrent generation efficiency at different blend ratios. As shown in Fig. 4b, the photocurrent generation of the devices based on PIDTT-TT:$PC_{71}BM$ was limited to wavelengths below 600 nm due to the wide band gap of PIDTT-TT (UV-Vis absorption spectra of the blend film is shown in Fig. S3†). The integrated J_{SC} values from the IPCE spectra are well matched with the J_{SC} measured under 1-sun illumination (within an error of 5%), and follow the same trend of J_{SC} change to the different blend ratios. The device with a 1 : 2 blend ratio exhibited the maximum IPCE value (up to 89%), indicating efficient photo-induced charge generation and charge carrier transport with the 1 : 2 blend ratio in the PIDTT-TT:$PC_{71}BM$ film.

As reported elsewhere, the introduction of processing additives can lead to further optimization of the BHJ morphology of the photoactive layer; this can significantly improve the PCE of PSCs. In order to further optimize the device performance, 1,8-diiodooctane (DIO), 1-chloronaphthalene (CN), and diphenyl ether (DPE) were added to the solution. All of the device parameters with different amounts of additives are listed in Table S1 in the ESI.† As shown in Fig. 4c and Table 1, all of the additives improved their device performance. Among these, the device with 2 vol% CN added to the blend exhibited the best J_{SC} (11.2 mA cm^{-2}) and FF (0.66), resulting in a champion PCE of 7.10% (average values are listed in Table 1). The statistics of PCE values of the devices under each condition are shown in Fig. S4.† Meanwhile, the devices with DIO and DPE also yielded positive effects, generating champion PCEs of 6.43% and 6.29%, respectively. However, they are inferior values compared to the PCE from the device with CN. The IPCE spectrum of the device with CN achieved a conversion efficiency of 89%, demonstrating that the ideal BHJ photoactive layer in which efficient exciton generation and charge transport are carried out was formed with CN as an additive (Fig. 4d). It would be noteworthy to mention that this is one of the highest values for PSCs based on wide band gap polymers with $E_g > 2.1$ eV to the best of our knowledge. In order to compare the device efficiency of PIDTT-TT with P3HT, a well-known wide band gap polymer, we also fabricated the devices using P3HT:$PC_{71}BM$ as an active layer. As presented in Fig. S5,† P3HT:$PC_{71}BM$-based devices exhibited a maximum PCE of 3.96% with a V_{OC} of 0.56 V, a J_{SC} of 10.41 mA cm^{-2} and a FF of 0.68 (Table 1). Thus, PIDTT-TT exhibited a *ca.* 79% improved PCE value compared to the P3HT-based device, suggesting the efficacy of PIDTT-TT for wide band gap polymers for solar cell applications.

We observed the blend film morphology of the photoactive layer by transmission electron microscopy (TEM). The BHJ photoactive layer cast from DCB formed a randomly mixed morphology of PIDTT-TT and $PC_{71}BM$ (Fig. 5a). The small domain size of the BHJ would be advantageous for efficient exciton dissociation. However, the presence of poorly connected, small domains and aggregate trap sites lowers the charge generation and transport in the photoactive layer of the device. This results in inferior J_{SC} and FF values in the device. After the additives are mixed into the solution, the domains of the BHJ photoactive layer become more discernible, generating a distinct fibril structure on the order of *ca.* 20–30 nm. It has also been reported that the optimal domain size for efficient exciton diffusion and dissociation is between 10 and 20 nm. In particular, the blend film processed with CN exhibited the most distinct nanostructures with well-interconnected networks. Thus, the PIDTT-TT:$PC_{71}BM$ blend processed with CN is

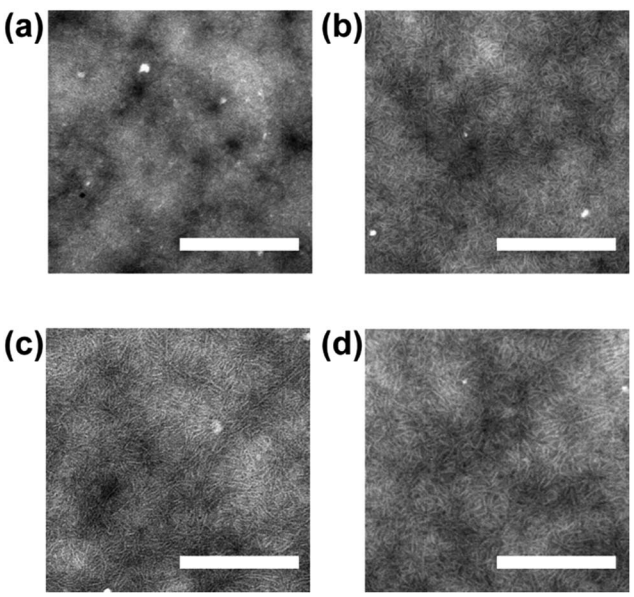

Fig. 5 TEM images of PIDTT-TT:$PC_{71}BM$ blend films cast from (a) DCB, (b) DCB/DIO, (c) DCB/CN and (d) DCB/DPE. The scale bar denotes 500 nm.

beneficial for the efficient generation of charge carriers, as reflected in the improved IPCE; this leads to the superior J_{SC} and FF of the devices, which combine to achieve a PCE that exceeds 7%.

Exciton dissociation and charge collection are mainly governed by the BHJ blend film morphology. We investigated the exciton dissociation/charge collection efficiencies of the devices by calculating the ratio of the photocurrent density (J_{ph}) to the saturation current density (J_{sat}) (J_{ph} at $V = 2$ V) under short-circuit conditions ($V = 0.96$ V for all devices) (Fig. 6a).[43] The J_{ph}/J_{sat} value for the device without the additives was 0.86, while the devices with the additives had ratios of 0.90, 0.93, and 0.91 for DIO, CN, and DPE, respectively. Clearly, the additives led to improved BHJ morphologies; thus, the photo-induced charge generation and collection were enhanced. In addition, the charge transport properties were also improved after the additives were used. As shown in Fig. S6,† the hole and electron mobilities of PIDTT-TT:$PC_{71}BM$ blends determined by the space-charge-limited current (SCLC) method were 1.75×10^{-4} and 6.42×10^{-5} cm^2 V^{-1} s^{-1} for DCB, 3.21×10^{-4} and 1.11×10^{-4} cm^2 V^{-1} s^{-1} for DCB/DIO, 7.18×10^{-4} and 4.05×10^{-4} cm^2 V^{-1} s^{-1} for DCB/CN and 3.50×10^{-4} and 2.18×10^{-4} cm^2 V^{-1} s^{-1} for DCB/DPE. This result also indicates that the well-developed interconnected BHJ morphology was caused after the additive was employed in the photoactive layer. We further investigated the maximum exciton generation rates (G_{max}) of the devices in order to understand the influence of blend film morphology on the J_{SC} variation. The G_{max} values of the devices studied in this work were estimated by plotting J_{ph} as a function of effective voltage (V_{eff}) ($J_{ph} = J_L - J_D$, where J_L and J_D are the current densities under illumination and dark conditions, respectively, and $V_{eff} = V_0 - V$, where V_0 is the voltage when $J_{ph} = 0$, and V is the applied voltage). As seen in Fig. 6a, J_{ph} was saturated as V_{eff} approached V. The G_{max} values of the devices were obtained from the equation of $J_{sat} = qLG_{max}$, where J_{sat} is the saturation photocurrent density, q is the electronic charge, and L is the thickness of the photoactive layer in the device. As a result, the devices processed with the additives generated enhanced G_{max} values compared to the DCB-based device (Table 1). This indicates that the photoactive layers processed with additives yielded improved photo-induced charge generation and collection.

To study the charge recombination quantitatively, the relationship between J_{SC} and the light intensity (P) was analysed (Fig. 6b). As is known, higher α values correspond to suppressed photocurrent losses due to bimolecular recombination from the power law equation of $J_{ph} \propto P^{\alpha}$, where α is a recombination parameter. Thus, the highest value for the device with the CN additive suggests that bimolecular recombination is considerably suppressed in the PIDTT-TT:$PC_{71}BM$ blend processed with CN. From the morphological and device investigations discussed above, it is concluded that the improved BHJ morphology, which was induced by the additives, allows better photo-induced charge generation, efficient charge transport/collection, and suppressed recombination. These factors combine to enhance the photovoltaic performance. In particular, CN was found to be the most effective additive for the PIDTT-TT:$PC_{71}BM$ blend film for the PSCs.

The device stability in long-term storage under ambient conditions is another important parameter for the practical application of PSCs. The ambient stability of PIDTT-TT:$PC_{71}BM$-based PSCs was investigated, as shown in Fig. 7. The PIDTT-TT-based device exhibited superior ambient stability, retaining

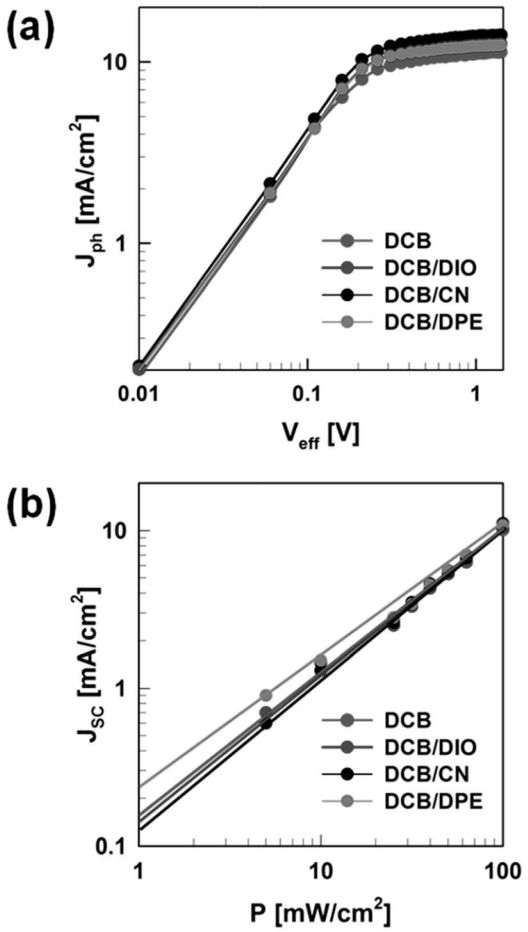

Fig. 6 (a) J_{ph}–V_{eff} curves and (b) J_{SC} dependence on the light intensity of the devices with different solvent additives.

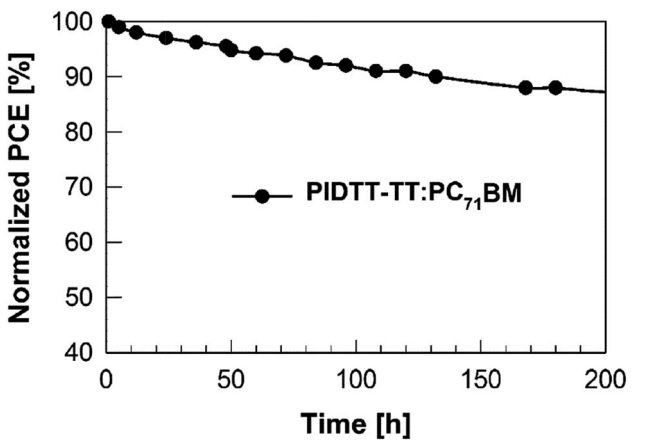

Fig. 7 Normalized PCE degradation of the devices based on PIDTT-TT:$PC_{71}BM$ and P3HT:$PC_{71}BM$ under exposure to ambient conditions.

>90% of its initial PCE after seven days of exposure to ambient conditions; this is significantly higher than that of the P3HT-based device. After 15 days of exposure to ambient conditions, the device made with PIDTT-TT still exhibited 65% of its initial PCE. The high ambient stability of the PIDTT-TT-based device can mainly be attributed to the deep HOMO level of the PIDTT-TT, which prevents oxidation of the conjugated polymer. Consequently, the PIDTT-TT would be a promising oxidation-resistant photoactive material for highly stable solar cells.

Conclusions

Herein, we demonstrated high-performance PSCs by designing a novel wide band gap conjugated polymer, PIDTT-TT, as a photoactive electron donor material. A judicious combination of IDTT and TT, which exhibits strong electron-donating capabilities, afforded a wide band gap (E_g = 2.14 eV) with intense light absorption in the UV-Vis range. Along with its wide band gap, PIDTT-TT showed deep energy levels, which favor higher V_{OC}s, serving to compensate for the limited photon harvesting of the device. The use of PIDTT-TT yielded an impressive PCE of 7.10%, along with high V_{OC} (0.96 V), FF (0.66), and IPCE (89%). This represents one of the highest PCEs for a PSC made with a wide band gap polymer (with a E_g > 2.1 eV). Another interesting feature is that the PIDTT-TT-based device exhibited high stability under ambient conditions. After exposure to ambient atmosphere for 15 days, the PCE decreased by only 17%, suggesting the high anti-oxidative capabilities of PIDTT-TT; this feature is attributed to its deep energy levels. Thus, it is concluded that PIDTT-TT is an interesting wide band gap conjugated polymer for use in high-performance PSCs. In addition, it should be a promising candidate as a short wavelength absorption polymer for tandem devices.

Acknowledgements

This research was supported by the Korea Institute of Industrial Technology (kitech-ER-16-010) and Basic Science Research Program through the National Research Foundation of Korea (NRF) funded by the Ministry of Education (NRF-2016R1C1B2006941).

Notes and references

1 Y. Liu, J. Zhao, Z. Li, C. Mu, W. Ma, H. Hu, K. Jiang, H. Lin, H. Ade and H. Yan, *Nat. Commun.*, 2014, **5**, 5293.
2 J. W. Jung, J. W. Jo, E. H. Jung and W. H. Jo, *Org. Electron.*, 2016, **31**, 149–170.
3 Z. C. He, C. M. Zhong, S. J. Su, M. Xu, H. B. Wu and Y. Cao, *Nat. Photonics*, 2012, **6**, 591–595.
4 J. You, L. Dou, K. Yoshimura, T. Kato, K. Ohya, T. Moriarty, K. Emery, C.-C. Chen, J. Gao, G. Li and Y. Yang, *Nat. Commun.*, 2013, **4**, 1446.
5 Y. Yang, W. Chen, L. T. Dou, W. H. Chang, H. S. Duan, B. Bob, G. Li and Y. Yang, *Nat. Photonics*, 2015, **9**, 190–198.
6 N. Wang, Z. Chen, W. Wei and Z. Jiang, *J. Am. Chem. Soc.*, 2013, **135**, 17060–17068.
7 Y. Li, *Acc. Chem. Res.*, 2012, **45**, 723–733.
8 G. Li, R. Zhu and Y. Yang, *Nat. Photonics*, 2012, **6**, 153–161.
9 S. Liu, P. You, J. Li, J. Li, C. S. Lee, B. S. Ong, C. Surya and F. Yan, *Energy Environ. Sci.*, 2015, **8**, 1463–1470.
10 L. Nian, W. Q. Zhang, N. Zhu, L. Liu, Z. Q. Xie, H. B. Wu, F. Wurthner and Y. G. Ma, *J. Am. Chem. Soc.*, 2015, **137**, 6995–6998.
11 H. Ma, H.-L. Yip, F. Huang and A. K.-Y. Jen, *Adv. Funct. Mater.*, 2010, **20**, 1371–1388.
12 H.-L. Yip and A. K.-Y. Jen, *Energy Environ. Sci.*, 2012, **5**, 5994–6011.
13 C. H. Duan, K. Zhang, C. Zhong, F. Huang and Y. Cao, *Chem. Soc. Rev.*, 2013, **42**, 9071–9104.
14 C.-Z. Li, C.-Y. Chang, Y. Zang, H.-X. Ju, C.-C. Chueh, P.-W. Liang, N. Cho, D. S. Ginger and A. K.-Y. Jen, *Adv. Mater.*, 2014, **26**, 6262–6267.
15 J. W. Jung, F. Liu, T. P. Russell and W. H. Jo, *Adv. Mater.*, 2015, **27**, 7462–7468.
16 S. Zhang, L. Ye and J. Hou, *Adv. Energy Mater.*, 2016, **6**, 1502529.
17 Z. He, B. Xiao, F. Liu, H. Wu, Y. Yang, S. Xiao, C. Wang, T. P. Russell and Y. Cao, *Nat. Photonics*, 2015, **9**, 174–179.
18 T. Xu and L. Yu, *Mater. Today*, 2014, **17**, 11–15.
19 L. Lu and L. Yu, *Adv. Mater.*, 2014, **26**, 4413–4430.
20 J. W. Jung, F. Liu, T. P. Russell and W. H. Jo, *Energy Environ. Sci.*, 2013, **6**, 3301–3307.
21 Z. Li, H. Lin, K. Jiang, J. Carpenter, Y. Li, Y. Liu, H. Hu, J. Zhao, W. Ma, H. Ade and H. Yan, *Nano Energy*, 2015, **15**, 607–615.
22 J. Wolf, F. Cruciani, A. E. Labban and P. M. Beaujuge, *Chem. Mater.*, 2015, **27**, 4184–4187.
23 J.-H. Kim, J. B. Park, I. H. Jung, A. C. Grimsdale, S. C. Yoon, H. Yang and D.-H. Hwang, *Energy Environ. Sci.*, 2015, **8**, 2352–2356.
24 J.-H. Kim, J. B. Park, F. Xu, D. Kim, J. Kwak, A. C. Grimsdaled and D.-H. Hwang, *Energy Environ. Sci.*, 2014, **7**, 4118–4131.
25 L. Lan, Z. Chen, Q. Hu, L. Ying, R. Zhu, F. Liu, T. P. Russell, F. Huang and Y. Cao, *Adv. Sci.*, 2016, **3**, 1600032.
26 J. B. You, L. T. Dou, Z. R. Hong, G. Li and Y. Yang, *Prog. Polym. Sci.*, 2013, **38**, 1909–1928.
27 J. W. Jung and W. H. Jo, *Adv. Funct. Mater.*, 2010, **20**, 2355–2363.
28 J. W. Jung, J. W. Jo and W. H. Jo, *Adv. Mater.*, 2011, **23**, 1782–1787.
29 S. H. Park, A. Roy, S. Beaupré, S. Cho, N. Coates, J. S. Moon, D. Moses, M. Leclerc, K. Lee and A. J. Heeger, *Nat. Photonics*, 2009, **3**, 297–302.
30 J. W. Jung, F. Liu, T. P. Russell and W. H. Jo, *Adv. Energy Mater.*, 2015, **5**, 1500065.
31 T. E. Kang, T. Kim, C. Wang, S. Yoo and B. J. Kim, *Chem. Mater.*, 2015, **27**, 2653–2658.
32 W. Zhang, Y. Han, X. Zhu, Z. Fei, Y. Feng, N. D. Treat, H. Faber, N. Stingelin, I. McCulloch, T. D. Anthopoulos and M. Heeney, *Adv. Mater.*, 2016, **28**, 3922–3927.

33 A.-C. Knall, R. S. Ashraf, M. Nikolka, C. B. Nielsen, B. Purushothaman, A. Sadhanala, M. Hurhangee, K. Broch, D. J. Harkin, J. Novák, M. Neophytou, P. Hayoz, H. Sirringhaus and I. McCulloch, *Adv. Funct. Mater.*, 2016, **26**, 6961–6969.
34 I. McCulloch, R. S. Ashraf, L. Biniek, H. Bronstein, C. Combe, J. E. Donaghey, D. I. James, C. B. Nielsen, B. C. Schroeder and W. Zhang, *Acc. Chem. Res.*, 2012, **45**, 714–722.
35 X. Zhang, H. Bronstein, A. J. Kronemeijer, J. Smith, Y. Kim, R. J. Kline, L. J. Richter, T. D. Anthopoulos, H. Sirringhaus, K. Song, M. Heeney, W. Zhang, I. McCulloch and D. M. DeLongchamp, *Nat. Commun.*, 2013, **4**, 2238.
36 W. Zhang, J. Smith, S. E. Watkins, R. Gysel, M. McGehee, A. Salleo, J. Kirkpatrick, R. S. Ashraf, T. Anthopoulos, M. Heeney and I. McCulloch, *J. Am. Chem. Soc.*, 2010, **132**, 11437–11439.
37 W. Zhang, Y. Han, X. Zhu, Z. Fei, Y. Feng, N. D. Treat, H. Faber, N. Stingelin, I. McCulloch, T. D. Anthopoulos and M. Heeney, *Adv. Mater.*, 2016, **28**, 3922–3927.
38 S. Holliday, J. E. Donaghey and I. McCulloch, *Chem. Mater.*, 2014, **26**, 647–663.
39 H.-H. Chang, C.-E. Tsai, Y.-Y. Lai, D.-Y. Chiou, S.-L. Hsu, C.-S. Hsu and Y.-J. Cheng, *Macromolecules*, 2012, **45**, 9282–9291.
40 J. J. Intemann, K. Yao, Y. X. Li, H. L. Yip, Y. X. Xu, P. W. Liang, C. C. Chueh, F. Z. Ding, X. Yang and X. Li, *Adv. Funct. Mater.*, 2014, **24**, 1465–1473.
41 Y.-X. Xu, C.-C. Chueh, H.-L. Yip, F.-Z. Ding, Y.-X. Li, C.-Z. Li, X. Li, W.-C. Chen and A. K.-Y. Jen, *Adv. Mater.*, 2012, **24**, 6356–6361.
42 Y.-X. Xu, C.-C. Chueh, H.-L. Yip, C.-Y. Chang, P.-W. Liang, J. J. Intemann, W.-C. Chen and A. K.-J. Jen, *Polym. Chem.*, 2013, **4**, 5220–5223.
43 J. W. Jung, T. P. Russell and W. H. Jo, *ACS Appl. Mater. Interfaces*, 2015, **7**, 13666–13674.